Optimization of Solar-Photocatalytic Degradation of Polychlorinated Biphenyls Using Photocatalyst ($Nd/Pd/TiO_2$) by Taguchi Technique and Detection by Solid Phase Nano Extraction

Piramoon, Shadi; Aberoomand Azar, Parviz*+; Saber Tehrani, Mohammad

Department of Chemistry, Science and Research Branch, Islamic Azad University, Tehran, I.R. IRAN

Sirwan Mohammadiazar

Department of Chemistry, Sanandaj Branch, Islamic Azad University, Sanandaj, I.R. IRAN

ABSTRACT: *$Nd/Pd/TiO_2$ photocatalyst has been synthesized in the presence of Hydroxyl Propyl Cellulose by sol-gel method with Titanium tetra isopropoxide as titanium precursor. Photocatalyst size and structure properties of the nano-catalyst have been determined by X-Ray Diffraction (XRD). It has contained the anatase phase in advance. The surface area is measured by the Brunauer, Emmett, and Teller (BET) method. The presence of Ti, Nd, and Pd in the nanostructure has been confirmed by EDX, equipped tool with SEM. Photocatalytic degradation of PCB-28 under solar light has been investigated by the Taguchi method with five factors such as the amount of HPC (g/g_{sol}), the percentage of Pd (%), the percentage of Nd (%), calcination temperature (°C) and calcination time (h). Under optimal conditions such as 0.003 of HPC (g/g_{sol}), 0.2 percentage of Pd (%), 0.2 percentage of Nd (%), 700°C of the calcination temperature, and 5 hours for the calcination time, the best desorption result monitored by Solid Phase Nano Extraction (SPNE) technique method before degradation process. By GC-ECD, complete degradation of PCBs was observed after solar irradiation in 14min, and no PCBs chromatogram was observed after this time.*

KEYWORDS: *Photocatalyst; Polychlorinated biphenyls; Solid-phase nano-extraction; Taguchi; Degradation.*

INTRODUCTION

Polychlorinated biphenyls (PCBs) are chemical compounds that were previously added as additives to industrial oils to improve the properties and performance of the oil. However, these compounds are resistant and biodegradable, which can have a negative effect on human health and the environment. These compounds are highly toxic, have high chemical stability, resistant to decomposition, bio-accumulation in water and soil for years,

***** *To whom correspondence should be addressed.*
+ E-mail: *parvizaberoomand@gmail.com*
1021-9986/2021/5/1541-1553 13/$/6.03

as they are fat-loving. They accumulate in biological cells and enter into the food chain. They have already created a major environmental challenge. Therefore, it is essential to remove them from the environment[1–5]. Titanium dioxide (TiO_2) nanoparticles are more widely used as photo-catalyst in this regard. Its strong photocatalytic properties such as high oxidation and high stability, along with other advantages such as lack of toxicity and availability of results in different optical activators to eliminate pollutants extensively in various fields, including water treatment and sterilization, removal of air pollution, and in solar cells[6–9]. There are several methods of synthesizing TiO_2 nanoparticles [10,11], but the sol-gel method has more advantages, such as low-temperature synthesis, no need for special equipment, high purity products, and ease in production. Electrons in the TiO_2 photocatalyst capacity layer are excited in the presence of ultraviolet light with a wavelength of less than 400 nm. One of the crucial problems of these nanoparticles is the high level of band gap energy TiO_2 (3.2 e.V) for the anatase isotope as a result of UV light excitation[12,13]. Therefore, many attempts have been made to improve the photocatalytic activity of TiO_2. Doping TiO_2 nanoparticles with metal and nonmetallic atoms by reducing the band gap can increase photocatalytic properties under visible light exposure[14–20]. The robust design of an engineering methodology is needed to optimize the process conditions of the product, so that the product and processor will be the smallest of the components involved and will result in high-quality products. One of the most critical powerful design tools is the design of the parameters by the Taguchi method. Among the total number of experiments in a complete factorial arrangement, the arrays are selected with specific features. Thus this technique with the use of Orthogonal Arrays (OA), dramatically reduces the number of experiments[21].

Many studies have been carried out by Doping TiO_2 with different metals[22–25], but the effect of doped Nd and Pd has not been studied simultaneously. This work describes the study of the photocatalytic activity of prepared Nd/Pd/TiO_2 with HPC for degradation of PCBs under solar light. Photocatalytic degradation of PCB-28 has been investigated by the Taguchi method with 5 factors, such as the amount of HPC (g/g_{sol}), the percentage of Pd (%), the percentage of Nd (%), calcination temperature (°C), calcination time (h), and finally optimization has been achieved. Also, the importance of this study is to investigate PCBs trace analysis by GC-ECD from µg/L to ng/L during degradation by reducing the presence of HPC in water. The Solid-Phase Nano Extraction (SPNE) technique has been utilized to extract PCBs from aqueous media.

EXPERIMENTAL SECTION

Materials

Titanium tetra-isopropoxide (TTIP) was obtained from Aldrich Chemical Co. (USA). HPC, Sodium chloride (NaCl), sodium hydroxide (NaOH), hydrochloric acid (HCl), and n-hexane were all of the analytical grades and were obtained from E.Merck (Germany). Carboxyl-Multi-Walled Carbon NanoTubes (CMWCNT, O.D., of 8-15nm, and lengths: 30-50 µm, Purity: 99.9%) was obtained from Neutrino, Inc. (USA). Neodymium Nitrate, Palladium (II) trifluoroacetate, and PCBs standard reference material mixture, including PCB-28, PCB-52, PCB-101, PCB-138, PCB-153, PCB-180 were all from Sigma-Aldrich.

Preparation of HPC synthesized Nd/Pd/TiO_2 catalysts

The solution was prepared based on the method of our earlier work[26], with the addition of metal solutions for doping. Different solutions with proper molar ratios were prepared as follows:

Solution A: TTIP was dissolved in ethanol in molar ratios of 1: 100, and HPC was added to the solution, stirred by homogenizer for 1h.

Solution B: HNO_3 / Ethanol / H_2O with the molar ratio: 0.15:23:1 homogenized in 1 min at 2000 rpm.

Solution C: Neodymium Nitrate / Palladium (II) trifluoroacetate / Ethanol / HNO_3 with molar ratio: 0.2:0.2:20:0.05 was prepared to make a metal ion solution.

The solution B was dropped slowly to solution A and homogenized at 1000rpm at room temperature. After that, solution C was added to it and pH was kept neutral. The resulting colloidal suspension was homogenized for 1h as the sample (TNPH), the same procedure also was used to prepare the sample (TNH) with the elimination of Palladium, and the sample (TPH) with the elimination of Neodymium in part C. Sample

(TNH) with elimination metals doping in part C were also prepared. The obtained colloidal suspensions were sonicated in the vicinity of an ultrasound system for 30min and then aged and dried in an oven for 24h. Afterward, the dry material was calcined in a Carbolite furnace (RHF- 1400) at the desired temperature.

Instrumentations

The catalyst was characterized by XRD (SCIFERT-3003 PTS X-ray diffractometer), Cu-Kα radiation from 2θ = 5-100º (θ = 1.5406) in steps of 0.05º to identify the structure. The specific surface area was determined by the Brunauer, Emmett, and Teller method, using analyzer equipment (Beijing JWGB Sci. &Tech., China). Morphology and particle size were observed by SEM-XL30 scanning electron microscope equipped with Energy-Dispersive X-ray spectroscopy (EDX). Thermo Nicolet Nexus 870FT-IR and Thermo Nicolet 960 FT-Raman both from the USA were used for FT-IR and FT-Raman spectra of the samples. A tabletop centrifuge (Sigma, 2-16KC; 12104, Angle rotor; Germany) was used for centrifugation. For detection of PCBs before and after degradation, a Perkin Elmer XL gas chromatograph equipped with an Electron Capture Detector (ECD) and the capillary column (phase, elite 5). GC conditions were followed as temperature programming: 70°C, ramp rate at 10°C min^{-1} to 300°C (10 min); hot needle injections (1.0 µL); injector temperature, 250°C; oven temperature 300°C; detector temperature 310 °C; split ratio, splitless; carrier gas, N_2 (1 mL/min); system software, TotalChrom Navigator (Perkin Elmer Instruments). The intermediate analysis was performed using a GC–mass spectrometry system (Polaris Q, Al/As 3000, Trace GC 2000). The column temperature was programmed to increase from 70 °C, ramp rate at 10°C/min to 280 °C (10 min); system software, Xcalibur (Thermo Electron Corporation).

Taguchi Design

Generally in designing experiments, the process variables are divided into control and non-controlling categories to find the optimal levels, parameter levels, and to determine their effectiveness. In Taguchi design, the Signal-to-Noise (S/N) ratio indicates the sensitivity of the qualitative feature examined to controlling and non-controlling factors in a controlled process for which, various orthogonal arrays are used as matrix tests based on the number of selected parameters and related levels [27]. In this method, the variation is introduced with a factor called the S/N ratio, and the experimental conditions, which have the highest S/N ratio, are selected as optimal conditions by Minitab 17 software.

The orthogonal arrays are given as L_n (XY), where n represents the number of experiments, X indicates the number of factor levels, and Y represents the maximum number of factors that can be examined with the array. In the standard method, with regard to the "bigger is better" model, the higher the response value and the lower the loss of quality, (S/N) is calculated using the equation:

$$S/N = -10 * \log(\sum(1/Y^2)/n)$$

Where *n* is the number of observations, *Y* is the result of the experiments[28]. In this study, photocatalytic degradation PCB-28 has been investigated by the Taguchi method with 5 factors, including the amount of HPC (g/g_{sol}), Percentage of Pd (%), Percentage of Nd (%), Calcination temperature (°C), and Calcination time (h) in 5 levels (Table 1). Regarding the input parameters and selectivity levels, the L_{25} orthogonal array was selected as the matrix of experiments.

Catalytic method for seawater during degradation

A simple batch photoreactor of 1L in volume was prepared for this work, the inner surfaces of the reactor was made of a mirror to increase the intensity of light (Fig.1). A magnetic stirrer device was used for continuous circulation. The reactor procedure was under solar light at 11 AM. Before irradiation suspensions of the catalyst, they were sonicated for 30min in order to uniform the catalyst particles. Clean seawater samples were obtained from the Persian Gulf, Kish island, during December. Photocatalytic degradation of the seawater was studied under the following conditions: the amount of the photocatalysts was 1.0 g/L; the pH of the seawater was almost 7.7; no PCBs congener was found by the SPNE analysis in it. The temperature was kept approximately at 25±0.5ºC by the water cooling jacket. After centrifugation, the desired samples (volume of each sample was 1000 µL) were taken out from the reactor for GC-ECD analysis during illumination.

Table 1: Levels and factors used in this experiment.

Number of levels	Amount of HPC (g/g_{sol})	Percentage of Pd (%)	Percentage of Nd (%)	Calcination temperature (°C)	Calcination time (h)
1	0.002	0.1	0.1	400	2
2	0.0025	0.2	0.2	500	3
3	0.003	0.4	0.4	600	4
4	0.0035	0.6	0.6	700	5
5	0.004	0.8	0.8	800	6

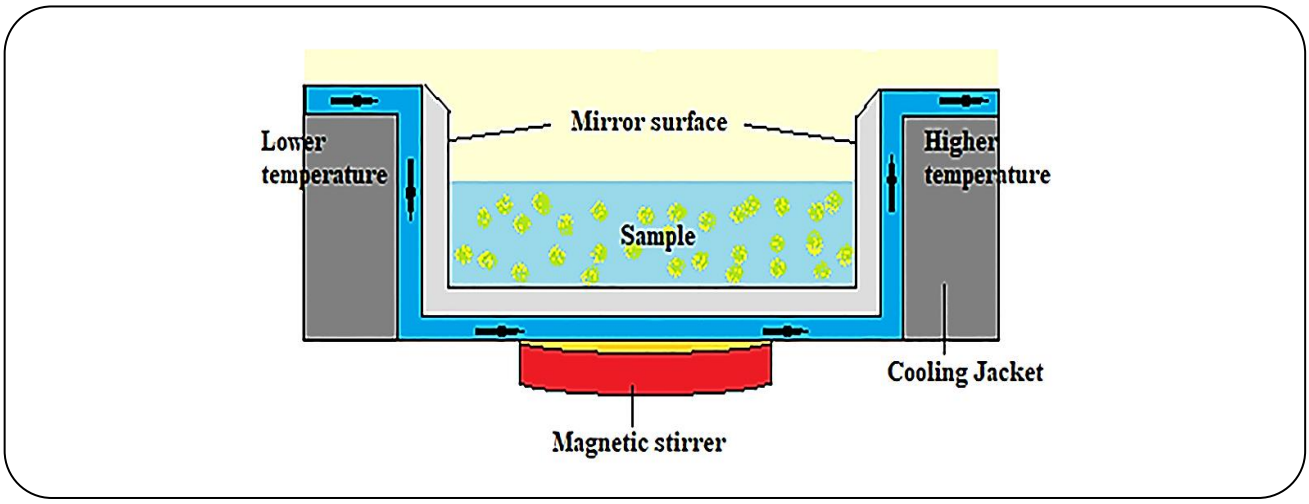

Fig. 1: The reactor. The type of inside walls is the mirror.

RESULTS AND DISCUSSION

Catalyst Characterization

The structural properties of the related synthesized catalysts are recorded in Table 2 according to the Debye–Scherrer equation, the HPC container sample (TNPH), possess 80.32% of anatase phase, 19.68% of Brookite phase, and no Rutile phase. The average particle size of prepared catalysts decreased to 21 nm with doping by Nd, Pd, and additive HPC. The Raman spectroscopy confirmed the formation of all of the expected anatase vibrational modes. As shown in Fig.2, the peaks observed at around 144.90, 249.58, 320.58, 398.92, 517.04, and 639.43 cm^{-1} are attributed to the anatase phase of TiO_2, and its crystalline structure was not changed by the doping procedure[29]. Raman spectra (Fig.2) and XRD (Fig.3) show no formation of the rutile phase in TNPH sample. FT-IR spectra of samples in the wave range number 400 - 4000 cm^{-1} are shown in Fig.4. A peak appearance at 3000-3600cm^{-1} is related to the absorption band of OH stretching vibration of surface hydroxyl group due to the use of ethanol during the synthesis. The absorption band observed around 1630cm^{-1} is due to the stretching mode of physical hydroxyl adsorption. The intensity of this peak is increased by the presence of dopants Pd and Nd in samples[30] which show the increase in surface OH groups. The peaks around 1115-1120 cm^{-1} are assigned to the asymmetric stretching vibration of the Ti-O bands. The absorption peak at 620cm^{-1} is assigned to Ti-O-Ti stretching motion. The peaks around 479, and 446cm^{-1} in samples (b), (c), and (d) could be assigned to the vibration modes of anatase phased O–Ti–O–Nd and O–Ti–O–Pd bands[31]. Also, the presence of Ti, Nd, and Pd is confirmed by EDX as shown in Fig.5. According to Fig.6 for SEM image, uniformity with the presence of dopant and HPC is increased with a significant decrease of particle size and agglomeration complexes.

Table 2: The structural properties of the synthesized catalysts.

Catalyst	% Anatase	% Rutile	% Brookite	[a]S.S.A.	[b]A.P.S.
TH	65.23	23.43	20.34	115	46
TNH	66	23	11	117	43
TPH	70.82	12.1	17.08	128	35
TNPH	80.32	0	19.68	135	21

[a] *Specific Surface Area (m^2g^{-1})*
[b] *Average Particle Size (nm)*

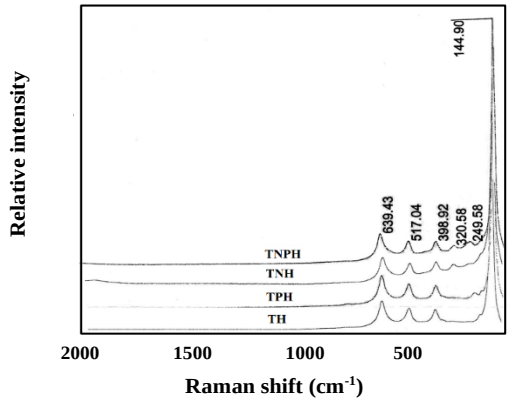

Fig. 2: Raman spectra of the prepared catalysts.

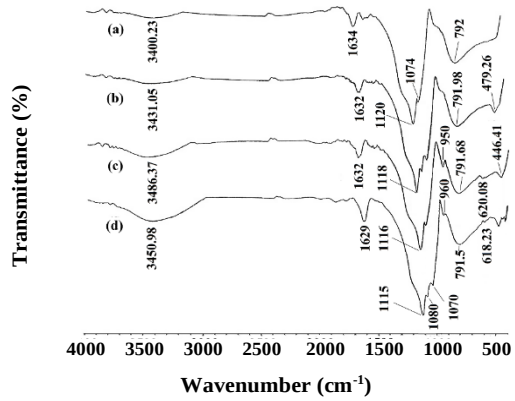

Fig. 4: IR spectra of prepared catalysts: a) TH, b) TNH, c) TPH, d) TNPH.

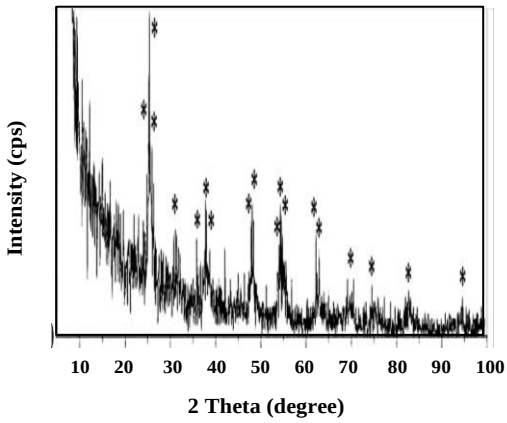

Fig. 3: X-ray diffraction patterns of TNPH photocatalyst synthesized by sol-gel method. *: Anatase phase.

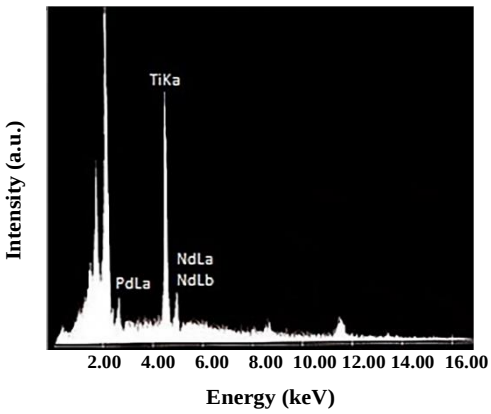

Fig. 5: Energy-dispersive X-ray diffraction (EDX) spectrum of TNPH photocatalyst synthesized by sol-gel method.

Effect of factors by Taguchi

In order to investigate the effect of varying factors and to optimize the process, the Taguchi method with L_{25} matrix was selected. The qualitative characteristic "bigger is better" was considered to set the aim. Besides, the S/N values of each invoice are shown in Table 3. For each factor, the most considerable value is reduced from the smallest one which is shown here as Delta in Table 4, the main effect of that factor is confirmed. Fig. 7 shows the main effects plot for each value, in which, the max point in each plot is better in response to the best photocatalytic effect. As shown in Table 4, the order effect of the factors follows as Calcination temperature (°c)> Calcination time (h)> Percentage of Pd (%)

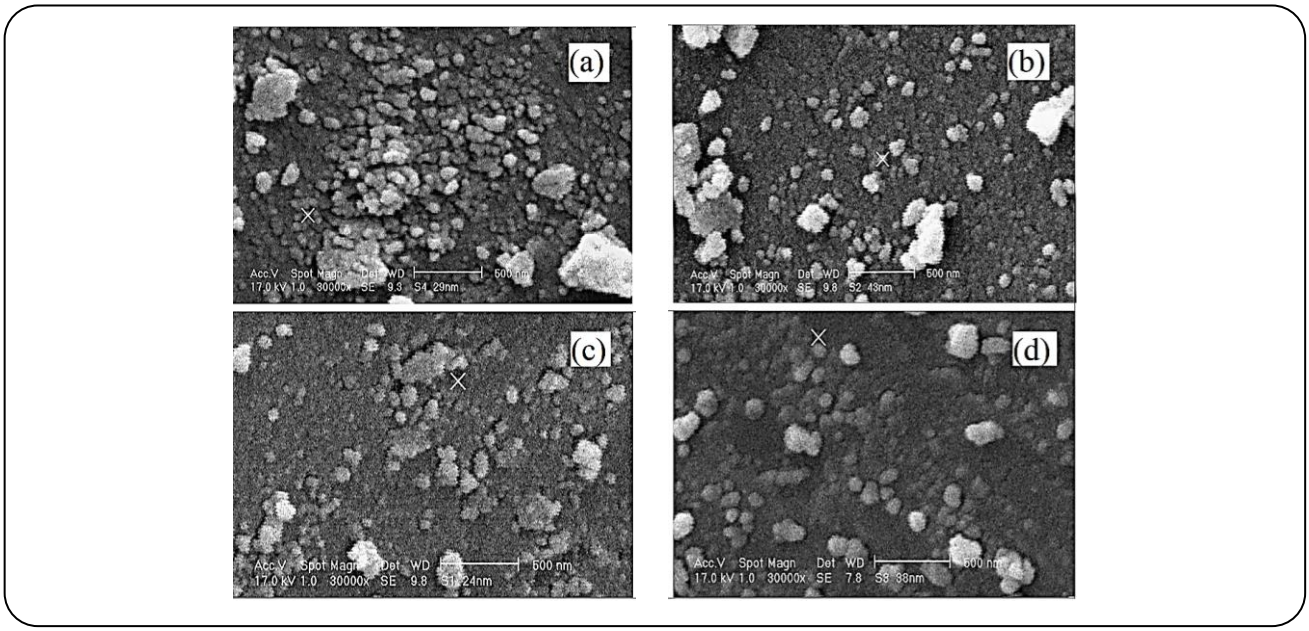

Fig. 6: SEM images of prepared catalysts: a) TH, b) TNH, c) TPH, d) TNPH.

>Percentage of Nd(%) >Amount of HPC (g/g_{sol}). Furthermore, Fig. 8 shows 3D scatterplot of S/N ratios of, A: calcination temperature (^0C) vs Nd (%) vs calcination time (h), B: calcination temperature (^0C) vs Pd (%) vs calcination time (h), C: calcination temperature (^0C) vs Pd (%) vs Nd (%)

Effect of different amounts of HPC

The presence of HPC during synthesis prevents agglomeration and particles stick together, this can affect the size of the particles and their performance[32]. In this study different amounts of HPC (0.0020, 0.0025, 0.0030, 0.0035, 0.0040 (g/g_{sol}) were studied. Based on the results obtained, the amount of HPC has the least effect on the photocatalytic degradation process. The best amount of HPC is obtained as 0.0030 (g/g_{sol}).

Effect of dopants percentage

Doping of intermediate metals leads to maximize on the photocatalytic activity of titanium[33,34]. The presence of a doped metallic ion in the Ti crystal network is strongly influenced by optical activity, the speed of the production of load carriers, and the electron transfer rate at the catalyst surface[35]. In a catalyst that is doped by the metal ion, the conduction band electrons easily recover an electron-type, and the layer cavities easily react as oxidization of electron species, so the percentage of catalytic activity for oxidation and reduction is increased. In this study, different weight percentages dopants of Nd and Pt (0.1, 0.2. 0.4, 0.6, 0.8) were studied. The results showed that for doped metal Nd and Pd, the highest efficiency is related to 0.2 of weight percent. The addition of metals to TiO_2 with HPC can facilitate the formation of the anatase phase at the temperature of 700°C. According to the results in Table 2, TNPH has the lowest Surface area, minimum particle size, and shortest time for PCB decomposition which means that by reducing the size of the particles of $Nd/Pd/TiO_2$, activity increases. As a result, due to the enhancement of the surface area, the number of active sites will rise, and as a result, the activity would increase.

Effect of temperature and time of calcination

The calcination temperature is very influential on important catalytic factors such as surface area, crystal size, anatase exchange ratio, and catalyst performance. In this study, the most effective factors in PCBs photocatalytic degradation are the temperature and calcination time of the catalyst. The temperature from 400-700ºC is studied. Calcination at 700ºC changed the phases to anatase in advance, which has resulted in a unique catalyst surface with increased photocatalytic activity.

Table 3: The L_{25} orthogonal array as the matrix of the experiments and S/N ratios.

Experiment number	Amount of HPC (g/g_{sol})	Percentage of Pd (%)	Percentage of Nd (%)	Calcination of temperature (°C)	Calcination of time (h)	Peak area (%)	S/N ratios
1	0.002	0.1	0.1	400	2	456321	113.185
2	0.002	0.2	0.2	500	3	747625	117.474
3	0.002	0.4	0.4	600	4	705539	116.97
4	0.002	0.6	0.6	700	5	780321	117.845
5	0.002	0.8	0.8	800	6	650046	116.259
6	0.0025	0.1	0.2	600	5	853215	118.621
7	0.0025	0.2	0.4	700	6	814793	118.221
8	0.0025	0.4	0.6	800	2	704567	116.958
9	0.0025	0.6	0.8	400	3	538532	114.624
10	0.0025	0.8	0.1	500	4	549643	114.802
11	0.003	0.1	0.4	800	3	758317	117.597
12	0.003	0.2	0.6	400	4	719642	117.142
13	0.003	0.4	0.8	500	5	724287	117.198
14	0.003	0.6	0.1	600	6	740655	117.392
15	0.003	0.8	0.2	700	2	780521	117.848
16	0.0035	0.1	0.6	500	6	709920	117.024
17	0.0035	0.2	0.8	600	2	675318	116.59
18	0.0035	0.4	0.1	700	3	750052	117.502
19	0.0035	0.6	0.2	800	4	789431	117.946
20	0.0035	0.8	0.4	400	5	675422	116.592
21	0.004	0.1	0.8	700	4	786054	117.909
22	0.004	0.2	0.1	800	5	890631	118.994
23	0.004	0.4	0.2	400	6	670521	116.528
24	0.004	0.6	0.4	500	2	624429	115.91
25	0.004	0.8	0.6	600	3	573214	115.166

Table 4: Response for S/N ratios (larger is better)

Number of levels	Amount of HPC (gg^{-1}_{sol})	Percentage of Pd (%)	Percentage of Nd (%)	Calcination of temperature (°C)	Calcination of time (h)
1	116.3	116.9	116.4	115.6	116.1
2	116.6	117.7	117.7	116.5	116.5
3	117.4	117	117.1	116.9	117
4	117.1	116.7	116.8	117.9	117. 9
5	116.9	116.1	116.5	117.6	117.1
Delta	1.1	1.6	1.3	2.3	1.8
*Rank	5	3	4	1	2

**: The order effect of the factors: Calcination of temperature (°c)> Calcination of time (h)> Percentage of Pd (%)>Percentage of Nd(%) >Amount of HPC (g/g_{sol})*

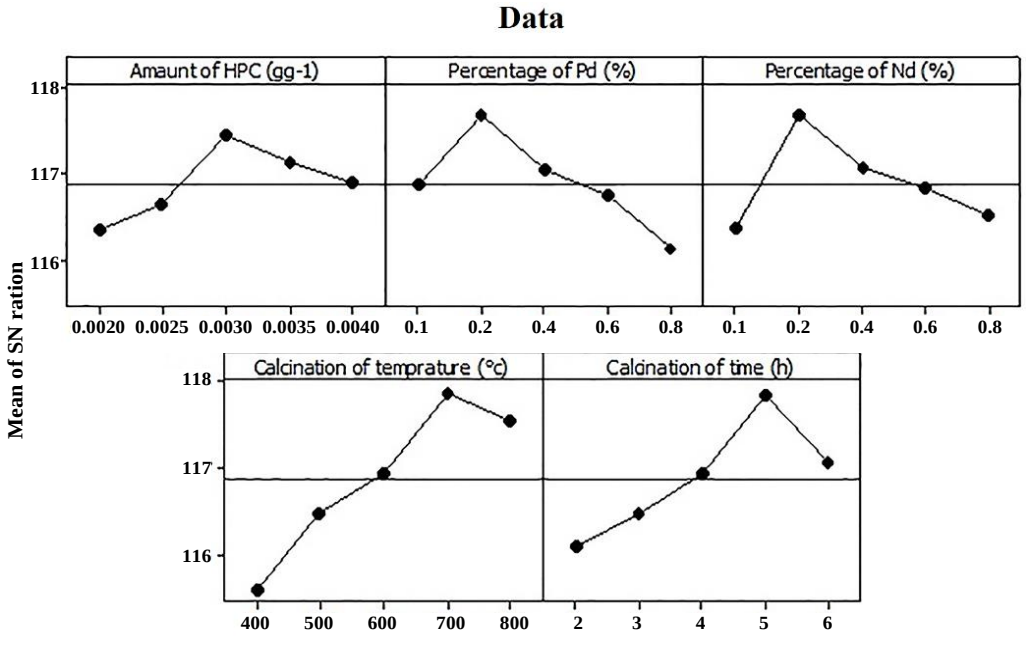

Fig. 7: Main effects plot for SN ratios(each value: HPC (g/g_{sol}), Percentage of Pd (%), Percentage of Nd (%), Calcination of temperature (°C) and Calcination of time (h)), signal to noise: larger is better.

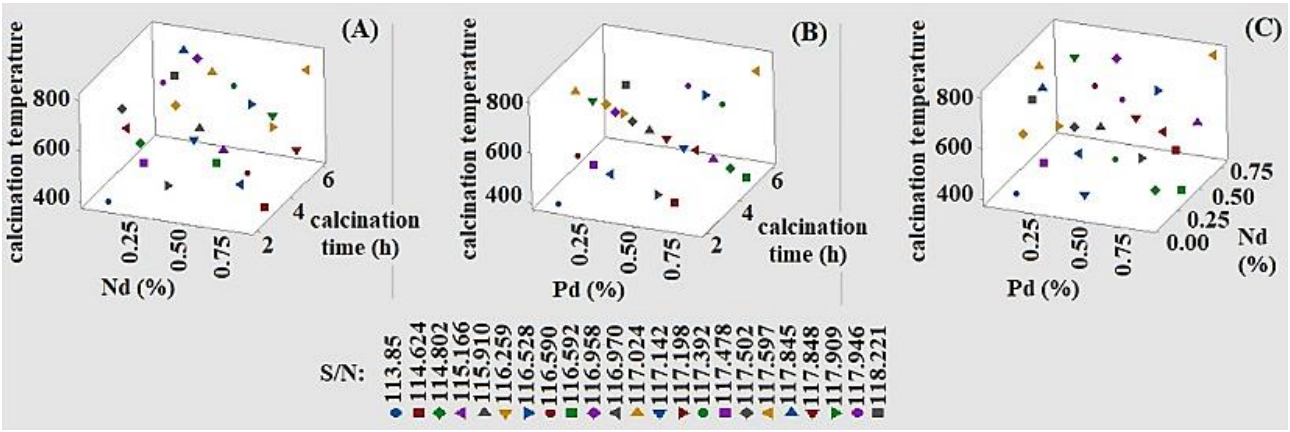

Fig. 8: 3D scatterplot of S/N ratios of, A: calcination temperature (^0C) vs Nd (%) vs calcination time (h), B: calcination temperature (^0C) vs Pd (%) vs calcination time (h), C: calcination temperature (^0C) vs Pd (%) vs Nd (%).

During calcination, the time of 5 h has the highest efficiency in photocatalytic degradation and consequently more anatase exchange phase in catalyst structure.

PCBs degradation and absent confirmation by the SPNE method

The photocatalytic degradation of PCBs by SPNE extraction is recorded in Fig. 9. The results show that no peak area was observed up to 14min. Spiked of 5µg/L was chosen as Maximum contamination because at higher levels, organic matter is further adsorbed on the surface of the molecular structure of the photocatalyst with a high concentration of pollutants. Therefore the photons are stopped before they can reach the catalyst level.

Therefore, the absorption of the photon by the catalyst is also reduced, and thus the percentage of degradation is also lowered [36]. For trace analysis of PCBs, SPNE extraction which is based on our earlier published

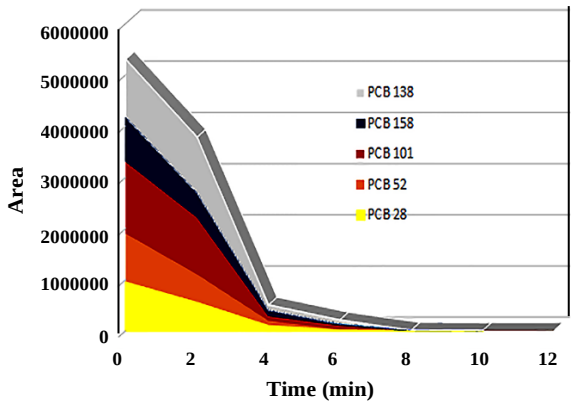

Fig. 9: Photocatalytic degradation; extraction condition: CNT (2mg), solution seawater 1mL, PCBs (5 µg/L), desorption solvent (20µL, n-Hexane), desorption time (5min).

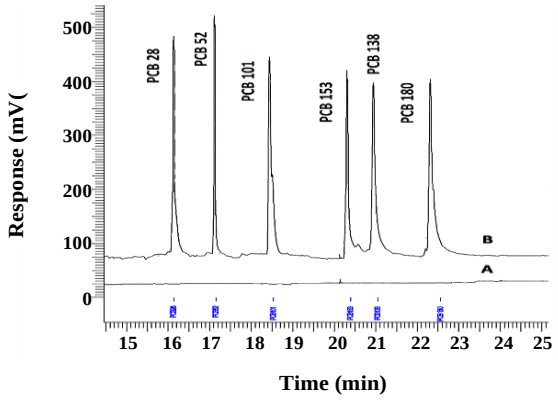

Fig. 10: Chromatogram of a) blank, b) 0.5 µg/L spiked seawater applying SPNE process.

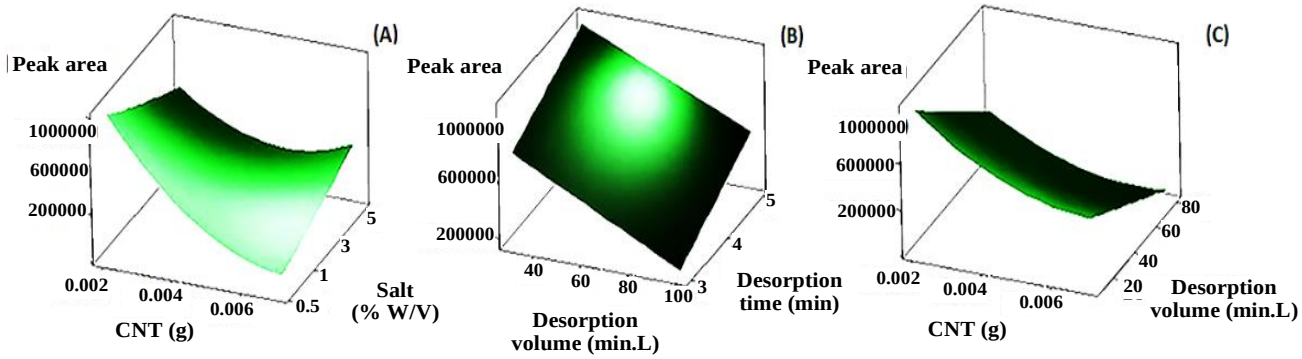

Fig. 11: 3D optimization plots of PCB-28, fixed values: (5µg/L max concentration, 1000 µL sample seawater, CMWCNT = 0.002 g; adsorption pH= 8, desorption pH= 7) with the hold values: (A) extraction time, 5min; desorption volume, 20 µL; desorption time, 5 min.

work [37], is utilized to confirm that no PCBs remained at the end of the photo-catalytic process. Briefly, 2 mg of CMWCNT as solid nano adsorbent weighted in micro-liter tubes with 1000 µL of filtered seawater either with or without degradation time. An ultrasonic bath was used for mixing in 5 min. The mixture was centrifuged at 8000 rpm for 2 min. Water phase decanted, and to avoid the presence of water in CMWCNT, a low flow of nitrogen-purged on it. 20 µL of n-Hexane is added to the solid phase residue for PCBs desorption from CMWCNT to the solvent. The mixture was first ultra-sounded, and then centrifuged again, and 1µL of the resulting supernatant was injected into GC-ECD. For monitoring PCBs, chromatographic peak areas were measured. First, the method was optimized at zero time of degradation without both solar light illumination and in the presence of the photo-catalyst. Adsorption and desorption conditions for SPNE carried out with 2 mg CMWCNT, PCBs (5µgL^{-1}), adsorption pH = 7-8, desorption pH = neutral). The SPNE optimization process was similar to our previous work, with the differences in the salt content, desorption solvent volume (n-Hexane) by the sample volume of 1000µL in seawater, and all were optimized. Based on the work, CMWCNT was selected as a nano sorbent because it affects the extraction efficiency due to the effective surface area and effective adsorption sites on it. This ascribes to the surface polarity of both biphenyl rings and the COOH group by π = π electron coupling as the electron donor and

Table 5: Concentration of each PCB congeners during degradation.

Time (min)	PCB 28 (C/C0) *100	PCB 52 (C/C0) *100	PCB 101 (C/C0) *100	PCB 153 (C/C0) *100	PCB 138 (C/C0) *100	PCB 180 (C/C0) *100
2	85.19%	85.96%	96.34%	94.77%	96.50%	94.23%
4	15.18%	15.34%	10.98%	15.70%	12.84%	10.20%
6	1.72%	1.75%	5.66%	5.75%	6.39%	5.36%
8	0.33%	0.34%	0.25%	0.19%	0.25%	0.21%
10	0.05%	0.06%	0.14%	0.03%	0.11%	0.14%
12	0.00%	0.00%	0.04%	0.00%	0.00%	0.01%
14	0.00%	0.00%	0.00%	0.00%	0.00%	0.00%

(C): concentration of each congener during illumination,
(C0): 5µg L^{-1} spiked initial concentration

interaction with chlorine groups of PCBs as the electron acceptor [37, 38]. Fig. 10 shows the Chromatogram of 0.5µgL^{-1} spiked seawater applying SPNE process. Fig. 11 illustrates 3D optimization plots of PCB-28 with the bold values mentioned in the picture. (A): extraction time, 5min; desorption volume, 20µL; desorption time, 5min. (B): extraction time, 5min; salt content, 0.5 (%W/V). (C): extraction time, 5min; salt content, 0.5 (%W/V); desorption time, 5min. Because of the presence of seawater, the salt content of 0.5% is enough for the salting-out effect, and 20µL of n-Hexane as desorption solvent volume were quite effective for SPNE extraction. To calculate the concentration of PCBs during degradation, first a calibration curve with peak area responses against concentrations of PCBs at seven points: 0.005, 0.01, 0.05, 0.1, 0.5, 1, and 5µg/L was plotted. For method validation, common factors such as correlation coefficient (R^2): 0.9986, RSD (n=3): ±7, LOD (S/N=3): 1.5 ng/L, LOQ (S/N=10): 4.9ng/L were calculated for PCB 28. The results show that after twelve minutes of degradation by the optimized photocatalyst; fewer PCB congeners remained in the matrix. Further, the final illuminated sample was analyzed by GC with a mass detector to confirm that the remained matrix is just water. Table 5 reports the presence percentage of each PCBs during the illumination process, (C) is the concentration of each congener during illumination, and (C0) is the 5µg /L initial concentration.

Photocatalytic degradation of 5µg/L spiked PCB

The photocatalytic degradation kinetic of PCB-28 was examined in the suspension. The percent degradation fitted a pseudo-first-order reaction model as:

$$\mathbf{Ln(C/C0) = -kt}$$

, and the half-life according to:

$$\mathbf{t_{1/2} = Ln(2)/k}$$

, where C0 and C are the concentrations of PCB-28 at an initial time and t- times, respectively. By plotting –Ln (C/C0) versus irradiation time (t), a linear behavior as pseudo-first-order kinetics for the photocatalytic degradation of 5µg/L spiked PCB-28 was obtained[39]. The $t_{1/2}$ of PCB-28 was 0.72 min with k of 0.94 min^{-1}, and the R-squared value (R^2) was obtained as 0. 997.

Intermediates of the photocatalytic degradation of PCBs

Photocatalytic degradation intermediates of PCB-28 were successfully obtained with 20 % acetone (v/v) extraction solution. The Retention Time (RT) of intermediates have appeared as 2-hydroxy-3-chlorobiphenyl, 6-hydroxy-3-chlorobiphenyl, 4, 4′-dichlorobiphenyl, and 2′-hydroxy- 2, 5-dichlorobiphenyl respectively. Apparently, the mechanism of photocatalytic degradation of PCB28 mainly involved dechlorination reactions and could be ascribed to the hydroxylation process in the semi-polar solution. The detailed mechanism of the whole PCB congeners is under investigation.

CONCLUSIONS

TiO_2 photocatalyst has been prepared in the presence of HPC by sol-gel method with TTIP as titanium precursor. Photocatalytic degradation of PCB-28 under solar light is investigated by the Taguchi method with five factors. Under optimal conditions,

0.003 HPC (gg^{-1}_{sol}), 0.2percentage of Pd (%), 0.2 percentage of Nd (%), calcination temperature 700°C, and calcination time 5h, Photocatalytic degradation of PCBs (5µg/L) was performed in 12 minutes under solar light illumination. The results show that calcination temperature had a high effect on the catalyst properties. PCBs extraction was utilized by SPNE method to confirm diminished concentrations during degradation. No PCBs congeners remained after 14min. Therefore, it can be concluded that Nd/Pd/TiO_2 is a suitable catalyst for the decomposition of PCBs congeners with high efficiency and short time for degradation under solar light. On the basis of simplicity, cost, and time-consuming in SPNE method, it is easy to use photocatalytic illumination detection for confirmation of organic pollutants in waters by GC-ECD.

Nomenclatures

ECD	Electron capture detector
CMWCNT	Carboxyl multi-walled carbon nanotubes
PCBs	Polychlorinated biphenyls
SPNE	Solid-phase nano-extraction method
HPC	Hydroxyl Propyl Cellulose
TNPH	TiO_2/Nd/Pd with HPC
TNH	TiO_2/Nd with HPC
TPH	TiO_2/Pd with HPC
TH	TiO_2 with HPC

CONFLICT OF INTEREST

The authors have declared no conflict of interest.

Received : Mar. 3, 2020 ; Accepted : July 6, 2020

REFERENCES

[1] Fan G., Wang Y., Fang G., Zhu X., Zhou D., Review of Chemical and Electrokinetic Remediation of PCBs Contaminated Soils and Sediments, *Environ. Sci. Process. Impacts.*, **18(9)**: 1140–1156 (2016).

[2] Shaban Y.A., El Sayed M.A., El Maradny A.A., Al Farawati R.K., Al Zobidi M.I., Khan S.U.M., Photocatalytic Removal of Polychlorinated Biphenyls (PCBs) Using Carbon-Modified Titanium Oxide Nanoparticles, *Appl. Surf. Sci.*, **365**: 108–113 (2016).

[3] Tang T., Zheng Z., Wang R., Huang K., Li H., Tao X., Dang Z., Yin H., Lu G., Photodegradation Behaviors of Polychlorinated Biphenyls in Methanol by UV-Irradiation: Solvent Adducts and Sigmatropic Arrangement, *Chemosphere.*, **193**: 861–868 (2018).

[4] Zhou Z., Zhang Y., Wang H., Chen T., Lu W., The Comparative Photodegradation Activities of Pentachlorophenol (PCP) and Polychlorinated Biphenyls (Pcbs) Using UV Alone and TiO_2-Derived Photocatalysts in Methanol Soil Washing Solution, *PLoS ONE.*, **9(9)**: 1–8 (2014).

[5] Zhu X., Wang Y., Qin W., Zhang S., Zhou D., Distribution of Free Radicals and Intermediates During The Photodegradation of Polychlorinated Biphenyls Strongly Affected by Cosolvents and TiO_2 Catalyst, *Chemosphere.*, **144**: 628–634 (2016).

[6] Bilal M., Ambreen B., Ali J., Shahid I., Adnan M., Hassan S., Ullah Khan A., Effects of Solvent on the Structure and Properties of Titanium Dioxide Nanoparticles and Their Antibacterial Activity, *Iran. J. Chem. Chem. Eng. (IJCCE)*, **38(4)**: 261-272 (2019).

[7] Janitabar Darzi S., Abdolmohammadi S., Latifi M., Green Removal of Toxic Th(IV) by Amino-Functionalized Mesoporous TiO_2-SiO_2 Nanocomposite, *Iran. J. Chem. Chem. Eng. (IJCCE)*, **39(2)**: 189-200 (2020).

[8] Shi H., Magaye R., Castranova V., Zhao J., Titanium Dioxide Nanoparticles: A Review of Current Toxicological Data, *Part. Fibre Toxicol.*, **10**: 1-15 (2013).

[9] Konstantinou I.K., Albanis T.A., TiO2-Assisted Photocatalytic Degradation of Azo Dyes in Aqueous Solution: Kinetic and Mechanistic Investigations: A Review, *Appl. Catal. B Environ.*, **49(1)**: 1–14 (2004).

[10] Huang Y., Zhou Q., Xiao J., Xie G., Determination of Trace Organophosphorus Pesticides in Water Samples with TiO_2 Nanotubes Cartridge Prior to GC-Flame Photometric Detection, *J. Sep. Sci.*, **33(14)**: 2184–2190 (2010).

[11] Liang P., Ding Q., Liu Y., Speciation of Chromium by Selective Separation and Preconcentration of Cr(III) on an Immobilized Nanometer Titanium Dioxide Microcolumn, *J. Sep. Sci.*, **29(2)**: 242–247 (2006).

[12] Zeng J., Peng C., Wang X., Wang R., Zhang N., Xiong S., One-Pot Self-Assembled TiO_2 /Graphene/Poly(acrylamide) Superporous Hybrid For Photocatalytic Degradation of Organic Pollutants, *J. Appl. Polym. Sci.*, **136(5)**: 47033 (2019).

[13] Saroj S., Singh L., Singh S.V., Photodegradation of Direct Blue-199 in Carpet Industry Wastewater Using Iron-Doped TiO_2 Nanoparticles and Regenerated Photocatalyst, *Int. J. Chem. Kinet.*, **51(3)**: 189–205 (2019).

[14] Lee H., Shin M., Lee M., Hwang Y.J., Photo-Oxidation Activities on Pd-Doped TiO_2 Nanoparticles: Critical PdO Formation Effect, *Appl. Catal. B Environ.*, **165**: 20–26 (2015).

[15] Akple M.S., Low J., Qin Z., Wageh S., Al-Ghamdi A.A., Yu J., Liu S., Nitrogen-Doped TiO_2 Microsheets With Enhanced Visible Light Photocatalytic Activity for CO_2 Reduction, *Chinese J. Catal.*, **36(12)**: 2127–2134 (2015).

[16] Mobtaker H.G., Malekinejad A., Yousefi T., Aghayan H., Studying the Photocatalytic Degradation of tri-n-butyl Phosphate Using Nano Nd-Doped TiO_2, *J. Sci. Islam. Repub. Iran.*, **28(1)**: 79–85 (2017).

[17] Mazur M., Wojcieszak D., Kaczmarek D., Domaradzki J., Zatryb G., Misiewicz J., Morgiel J., Effect of the Nanocrystalline Structure Type on the Optical Properties of TiO_2:Nd (1 at.%) Thin Films, *Opt. Mater. (Amst).*, **42**: 423–429 (2015).

[18] Momeni M.M., Ghayeb Y., Ghonchegi Z., Fabrication and Characterization of Copper Doped TiO_2 Nanotube Arrays by in Situ Electrochemical Method as Efficient Visible-Light Photocatalyst, *Ceram. Int.*, **41(7)**: 8735–8741 (2015).

[19] Yurdakal S., Tek B.S., Değirmenci Ç., Palmisano G., Selective Photocatalytic Oxidation of Aromatic Alcohols in Solar-Irradiated Aqueous Suspensions of Pt, Au, Pd and Ag loaded TiO_2 Catalysts, *Catal. Today.*, **281**: 53–59 (2017).

[20] Ou H.H., Lo S.L., Effect of Pt/Pd-Doped TiO_2 on the Photocatalytic Degradation of Trichloroethylene, *J. Mol. Catal. A Chem.*, **275(1–2)**: 200–205 (2007).

[21] Zhang L., Yao Q., Ma Y., Sun B., Shao C., Zhou T., Wang Y., Selim F. A., Wong C.P., Chen H., Taguchi Method Assisted Multiple Effects Optimization on Optical and Luminescence Performance of Ce: YAG Transparent Ceramics for High Power White LEDs, *J. Mater. Chem. C.*, **7**: 11431-11440 (2019).

[22] Kojima Y., Fukui M., Tanaka A., Hashimoto K., Kominami H., Additive-Free Semihydrogenation of an Alkynyl Group to an Alkenyl Group over Pd−TiO_2 Photocatalyst Utilizing Temporary In-situ Deactivation, *ChemCatChem.*, **10(16)**: 3605-3611 (2018).

[23] Feng Y., Hu X., Zhao F., Zeng B., Fe_3O_4/Reduced Graphene Oxide-Carbon Nanotubes Composite for the Magnetic Solid Phase Extraction and HPLC Determination of Sulfonamides in Milk, *J. Sep. Sci.*, **42**: 1058–1066 (2019).

[24] Palukuru P., Devangam A. V., Behara D. N., S-Codoped TiO_2/Fe_2O_3 Heterostructure Assemblies for Electrochemical Degradation of Crystal Violet Dye, *Iran. J. Chem. Chem. Eng. (IJCCE)*, **39(2)**: 169-177 (2020).

[25] Li L., Chang W., Wang Y., Ji H., Chen C., Ma W., Zhao J., Rapid, Photocatalytic, And Deep Debromination Of Polybrominated Diphenyl Ethers on Pd-TiO_2: Intermediates and Pathways, *Chem. - A Eur. J.*, **20(35)**: 11163–11170 (2014).

[26] Aberoomand Azar P., Moradi S., Piramoon S., Mashinchian A., Photocatalytic Degradation of Diazinon from Marine Source Using TiO_2 / SiO_2 Thin Layer Coated on Glass, *Int. J. Mar. Sci. Eng.*, **1(1)**: 23–28 (2011).

[27] Rahmani M., Kaykhaii M., Sasani M., Application of Taguchi L16 Design Method for Comparative Study of Ability of 3A Zeolite in Removal of Rhodamine B and Malachite Green from Environmental Water Samples, *Spectrochim. Acta - Part A Mol. Biomol. Spectrosc.*, **188**: 164–169 (2018).

[28] Sardar S., Karmakar S.K., Das D., Evaluation of Abrasive Wear Resistance of Al_2O_3/7075 Composite by Taguchi Experimental Design Technique, *Trans. Indian Inst. Met.*, **71**(8): 1847–1858 (2018).

[29] Sojić D.V., Despotović V.N., Abazović N.D., Comor M.I., Abramović B.F., Photocatalytic Degradation of Selected Herbicides in Aqueous Suspensions of Doped Titania Under Visible Light Irradiation, *J. Hazard. Mater.*, **179(1-3)**: 49–56 (2010).

[30] Kuvarega A.T., Krause R.W.M., Mamba B.B., Nitrogen/Palladium-Codoped TiO_2 for Efficient Visible Light Photocatalytic Dye Degradation, *J. Phys. Chem. C.*, **115(45)**: 22110–22120 (2011).

[31] Li J., Liu T., Sui G., Zhen D., Photocatalytic Performance of a Nd–SiO_2–TiO_2 Nanocomposite for Degradation of Rhodamine B Dye Wastewater, *J. Nanosci. Nanotechnol.*, **15(2)**: 1408–1415 (2015).

[32] Azar P.A., Dehaghi S.M., Samadi S., Tehrani M.S., Givianrad M.H., Effect of CMC and HPC mixture on the Photocatalytic Activity of Nd-TiO_2/SiO_2 Film under Visible Light Irradiation, *Turk. J. Chem.*, **35(1)**: 37–44 (2011).

[33] Zangiabadi M., Shamspur T., Saljooqi A., Mostafavi A., Evaluating the Efficiency of the GO-Fe_3O_4/TiO_2 Mesoporous Photocatalyst for Degradation of Chlorpyrifos Pesticide under Visible Light Irradiation, *Appl. Organomet. Chem.*, **33(5)**: e4813 (2019).

[34] Ding R.C., Fan Y.Z., Wang G.S., High Efficient Cu2O/TiO2 Nanocomposite Photocatalyst to Degrade Organic Pollutant under Visible Light Irradiation, *ChemistrySelect.*, **3(6)**: 1682–1687 (2018).

[35] Wang C., Zhan Y., Wang Z., TiO_2, MoS_2, and TiO_2/MoS_2 Heterostructures for Use in Organic Dyes Degradation, *ChemistrySelect.*, **3(6)**: 1713–1718 (2018).

[36] Daneshvar N., Aber S., Dorraji M.S.S., Khataee A.R., Rasoulifard M.H., Photocatalytic degradation of the Insecticide Diazinon in the Presence of Prepared Nanocrystalline ZnO Powders under Irradiation of UV-C Light, *Sep. Purif. Technol.*, **58(1)**: 91–98 (2007).

[37] Piramoon S., Aberoomand Azar P., Saber Tehrani M., Mohammadiazar S., Tavassoli A., Solid-Phase Nanoextraction of Polychlorinated Biphenyls in Water and Their Determination by Gas Chromatography with Electron Capture Detector, *J. Sep. Sci.*, **40(2)**: 449-457 (2017).

[38] Taha M.R., Mobasser S., Adsorption of DDT and PCB by Nanomaterials from Residual Soil, *PLoS ONE.*, **10(12)**: 1–16 (2015).

[39] Huang I.W., Hong C.S., Bush B., Photocatalytic Degradation of PCBs in TiO_2 Aqueous Suspensions, *Chemosphere.*, **32(9)**: 1869–1881 (1996).